Suv4-20h deficiency results in telomere elongation and derepression of telomere recombination

Roberta Benetti,[1] Susana Gonzalo,[1,3] Isabel Jaco,[1] Gunnar Schotta,[2] Peter Klatt,[1] Thomas Jenuwein,[2] and María A. Blasco[1]

[1]Telomeres and Telomerase Group, Molecular Oncology Program, Spanish National Cancer Centre, Madrid E-28029, Spain
[2]Research Institute of Molecular Pathology, Vienna Biocenter, A-1030 Vienna, Austria
[3]Radiation and Cancer Biology Division, Department of Radiation Oncology, Washington University School of Medicine, St. Louis, MO 63108

Mammalian telomeres have heterochromatic features, including trimethylated histone H3 at lysine 9 (H3K9me3) and trimethylated histone H4 at lysine 20 (H4K20me3). In addition, subtelomeric DNA is hypermethylated. The enzymatic activities responsible for these modifications at telomeres are beginning to be characterized. In particular, H4K20me3 at telomeres could be catalyzed by the novel Suv4-20h1 and Suv4-20h2 histone methyltransferases (HMTases). In this study, we demonstrate that the Suv4-20h enzymes are responsible for this histone modification at telomeres. Cells deficient for Suv4-20h2 or for both Suv4-20h1 and Suv4-20h2 show decreased levels of H4K20me3 at telomeres and subtelomeres in the absence of changes in H3K9me3. These epigenetic alterations are accompanied by telomere elongation, indicating a role for Suv4-20h HMTases in telomere length control. Finally, cells lacking either the Suv4-20h or Suv39h HMTases show increased frequencies of telomere recombination in the absence of changes in subtelomeric DNA methylation. These results demonstrate the importance of chromatin architecture in the maintenance of telomere length homeostasis and reveal a novel role for histone lysine methylation in controlling telomere recombination.

Introduction

Telomeres are nucleoprotein structures that protect the ends of chromosomes (Chan and Blackburn, 2002). A proper protective function of telomeres is accomplished by maintaining a minimum length of TTAGGG repeats as well as by the association of telomere-binding factors (for review see de Lange, 2005). Maintenance of telomere length homeostasis is primarily achieved by telomerase, a reverse transcriptase that adds telomeric repeats de novo after each cell duplication cycle, counteracting the end replication problem (Chan and Blackburn, 2002). Alternative ways to maintain telomere length have also been described, such as the so-called alternative lengthening of telomeres (ALT) mechanism, which is considered to rely on recombination among telomeric sequences (Dunham et al., 2000).

Recent evidence indicates that epigenetic modifications of the chromatin are also important to maintain telomere length homeostasis (Blasco, 2007). In particular, alterations in histone methylation or DNA methylation leading to the loss of heterochromatic features at telomeric and subtelomeric chromatin have been shown to result in telomere length deregulation (Blasco, 2005, 2007). Two of the main histone marks at compacted heterochromatin domains are the trimethylation of H3K9 and H4K20 as well as binding of the heterochromatin protein 1 isoforms (Lachner et al., 2001; Peters et al., 2001; Schotta et al., 2004). Cells lacking the Suv39h1 and Suv39h2 histone methyltransferases (HMTases) show decreased H3K9 trimethylation at telomeres concomitant with aberrant telomere elongation (Garcia-Cao et al., 2004). Similarly, mouse embryonic stem (ES) cells deficient for the DNA methyltransferases Dnmt1 or Dnmt3a,3b present a marked reduction in DNA methylation at subtelomeric domains, which is accompanied by dramatically elongated telomeres (Gonzalo et al., 2006). Furthermore, mouse embryonic fibroblasts (MEFs) lacking all three members of the Retinoblastoma family of tumor suppressors (Rb, p107, and p130) show decreased levels of H4K20 trimethylation at telomeres as well as a global reduction in DNA methylation, which again are concomitant with aberrant telomere elongation (Garcia-Cao et al., 2002; Gonzalo et al., 2005). These findings lead to the notion that a compacted or heterochromatic state at telomeres is

R. Benetti, S. Gonzalo, and I. Jaco contributed equally to this paper.

Correspondence to María A. Blasco: mblasco@cnio.es

Abbreviations used in this paper: ALT, alternative lengthening of telomeres; APB, ALT-associated PML body; ChIP, chromatin immunoprecipitation; dn, double null; ES, embryonic stem; HMTase, histone methyltransferase; MEF, mouse embryonic fibroblast; PML, promyelocytic leukaemia; PNA, peptide nucleic acid; Q-FISH, quantitative FISH; SCE, sister chromatid exchange; TRF, terminal restriction fragment; T-SCE, telomere SCE.

The online version of this article contains supplemental material.

The Journal of Cell Biology, Vol. 178, No. 6, September 10, 2007 925–936
http://www.jcb.org/cgi/doi/10.1083/jcb.200703081

required for a proper telomere length control (Blasco, 2005, 2007). However, more studies are needed to identify the different activities that participate in the assembly and regulation of telomeric chromatin as well as the mechanisms by which epigenetic alterations lead to telomere length deregulation.

In particular, the recently discovered Suv4-20h1 and Suv4-20h2 HMTases are prime candidates to carry the trimethylation of H4K20 at telomeres, as suggested by their ability to trimethylate H4K20 as well as to interact with heterochromatin protein 1 (Kourmouli et al., 2004; Schotta et al., 2004). In addition, the fact that all Rb family members can bind in vitro to Suv4-20h HMTases (Gonzalo et al., 2005) also suggests that these enzymes are responsible for H4K20 trimethylation both at pericentric and telomeric heterochromatin domains. In fact, evidence of their involvement on pericentric heterochromatin assembly has been already provided (Kourmouli et al., 2004; Schotta et al., 2004). However, direct evidence for a role of these enzymes on telomere chromatin architecture and regulation has been unknown to date.

With the goal of unraveling the enzymatic activities that participate in the assembly of telomeric chromatin structure and their mechanism of action, we assessed whether Suv4-20h1 and Suv4-20h2 HMTases are directly responsible for trimethylating H4K20 at telomeres and subtelomeres. For this, we used MEFs and ES cells deficient in either Suv4-20h1 (Suv4-20h1$^{-/-}$ MEF) or Suv4-20h2 (Suv4-20h2$^{-/-}$ MEF) or simultaneously deficient for both enzymes (Suv4-20h double-null [dn] MEFs and ES cells; see Cell culture section in Materials and methods). The results presented here show that abrogation of these enzymes results in decreased H4K20me3 at telomeric and subtelomeric domains concomitant with an increase in telomere length and in sister chromatid recombination both globally (sister chromatid exchanges [SCEs]) as well as at telomeric regions (telomere SCEs [T-SCEs]). In contrast, other heterochromatic marks at telomeres such as H3K9me3 and heterochromatin protein 1 binding were unaltered by the loss of these enzymes. In summary, we demonstrate that Suv4-20h HMTases actively participate in the correct assembly of telomeric chromatin and that their abrogation impacts telomere length homeostasis as well as telomere integrity.

Results

Abrogation of Suv4-20h HMTases results in telomere length deregulation

The two main histone marks characteristic of telomeric and subtelomeric heterochromatin are the trimethylation of H3K9 and the trimethylation of H4K20 (Garcia-Cao et al., 2002, 2004; Gonzalo et al., 2005, 2006). The mammalian enzymes responsible for the trimethylation of H3K9 at telomeres are the Suv39h1 and Suv39h2 HMTases (Garcia-Cao et al., 2004). However, the enzymes responsible for the trimethylation of H4K20 at telomeres have not been identified yet. To test whether the Suv4-20h1 and Suv4-20h2 HMTases are responsible for the trimethylation of H4K20 at telomeres, we studied telomeric chromatin in MEFs deficient in Suv4-20h1 or Suv4-20h2 or simultaneously deficient for both enzymes (Suv4-20h dn cells).

First, we measured the length of TTAGGG repeats using Southern blot terminal restriction fragment (TRF) analysis in Suv4-20h1$^{-/-}$, Suv4-20h2$^{-/-}$, and Suv4-20h dn MEFs derived from two different embryos of each genotype (see TRF analysis section in Materials and methods). As shown in Fig. 1 A, subtelomeric digestion with MboI released TRF fragments of higher molecular weight in Suv4-20h2$^{-/-}$ and Suv4-20h dn cells than in wild-type cells, indicating telomeres of greater length. In contrast, Suv4-20h1$^{-/-}$ cells did not show increased telomere length compared with the wild-type controls (Fig. 1 A). In agreement with the fact that these TRF fragments corresponded to telomeric sequences, they were digested with the Bal31 exonuclease (Fig. 1 B), which degrades DNA from the chromosome ends. We also confirmed elongated telomeres in Suv4-20h dn ES cells compared with the corresponding wild-type controls (Fig. 1 B). Of note, telomeres were slightly longer in ES cells compared with MEFs of the same genotype (Fig. 1 B), which is in agreement with the fact that they have higher telomerase activity and correspond to a more primitive developmental stage.

The long-telomere phenotype associated with Suv4-20h deficiency was confirmed by quantitative FISH (Q-FISH) of metaphase nuclei using a telomere-specific peptide nucleic acid (PNA) probe, which specifically measures the length of TTAGGG repeats at all individual chromosome ends (see Q-FISH analysis section in Materials and methods). Again, Suv4-20h2$^{-/-}$ and Suv4-20h dn MEFs presented significantly elongated telomeres of 36.5 $\pm$ 17.0 kb and 37.4 $\pm$ 17.7 kb, respectively, compared with 33.6 $\pm$ 17.2 kb in the wild-type controls ($P < 0.001$; Wilcoxon rank-sum test; Fig. 1 C). This was in contrast to Suv4-20h1$^{-/-}$ MEFs that showed similar length or slightly shorter telomeres compared with the wild-type controls (Wilcoxon rank-sum test; $P < 0.008$; Fig. 1 C). In agreement with elongated telomeres in Suv4-20h2$^{-/-}$ and Suv4-20h dn MEFs, these cells also showed a statistically significant higher percentage of telomeres longer than 50 kb and a lower percentage of telomeres shorter than 20 kb compared with the wild-type controls (χ^2 test; $P < 0.001$ for all comparisons with wild-type MEFs; Fig. 1 C).

Interestingly, telomere length deregulation in Suv4-20h2$^{-/-}$ and Suv4-20h dn MEFs did not result in increased chromosomal aberrations involving telomeric repeats as detected by Q-FISH (see Fig. 2 A for representative examples of chromosomal aberrations and Fig. 2 B for quantification), suggesting that these abnormally elongated telomeres retain a normal ability to protect chromosome ends from end to end fusion events. Altogether, these results indicate that simultaneous loss of the HMTase Suv4-20h1 and Suv4-20h2 activities results in a considerable telomere elongation in the absence of the loss of telomere capping.

Abrogation of Suv4-20h HMTases results in decreased H4K20me3 at telomeric chromatin

To test whether Suv4-20h HMTases are responsible for H4K20me3 at telomeres, we performed chromatin immunoprecipitation (ChIP) with antibodies recognizing this modification in cells that lack either Suv4-20h1, Suv4-20h2, or both h1 and h2 HMTases.

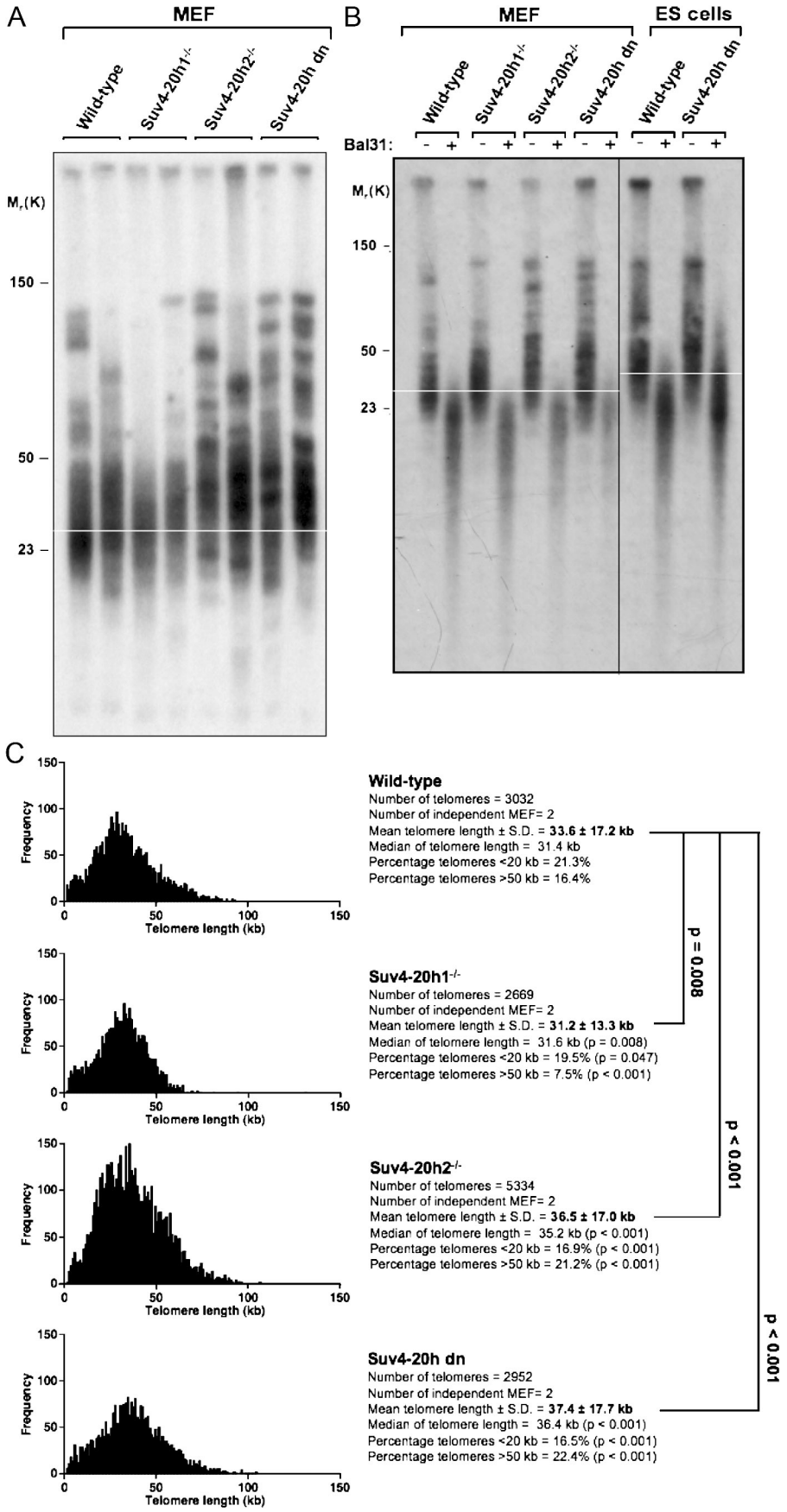

Figure 1. **Deregulation of telomere length in MEFs deficient for Suv4-20h HMTases.** (A) TRF results obtained with MEFs derived from two embryos of each of the wild-type, Suv4-20h1$^{-/-}$, Suv4-20h2$^{-/-}$, and Suv4-20h dn genotypes. Note the increased TRF size in Suv4-20h2$^{-/-}$ and Suv4-20h dn MEFs corresponding to longer telomeres. A white line is shown to facilitate the comparison of TRF sizes between different genotypes. (B) TRF results obtained with the indicated MEFs or ES cells, which were pretreated (+) or not pretreated (−) with Bal31 exonuclease. Note that TRF fragments are degraded upon Bal31 treatment, which is in agreement with the notion that they correspond to telomeric fragments. Note the increased TRF size in Suv4-20h dn MEFs and ES cells compared with the wild-type and Suv4-20h1$^{-/-}$ genotypes. A white line is shown to facilitate the comparison of TRF sizes between different genotypes. (C) Telomere length distribution of wild-type, Suv4-20h1$^{-/-}$, Suv4-20h2$^{-/-}$, and Suv4-20h dn MEFs as determined by Q-FISH. Two MEF cultures of each genotype were analyzed. A significant increase in mean telomere length is observed in Suv4-20h2$^{-/-}$ and Suv4-20h dn MEFs. Mean telomere length ± SD is indicated in bold characters. The total number of telomeres analyzed as well as the percentage of telomeres <20 kb and >50 kb are indicated. Statistical significance is calculated using the Wilcoxon rank-sum test. P-values are indicated in the figure.

Figure 2. **Detailed karyotyping analysis of Suv4-20h–deficient MEFs.** (A) Representative examples of the indicated chromosomal aberrations (indicated by yellow arrows) after chromosome orientation FISH (see Materials and methods). Blue, DAPI; green, leading telomere; red, lagging telomere. (B) Quantification of the frequency of chromosomal aberrations per metaphase in the indicated genotypes. Two independent MEF cultures were analyzed per genotype. The number of metaphases and the number of chromosomes analyzed per genotype are indicated. Numbers in parentheses correspond to the absolute number of aberrations detected in the indicated numbers of metaphases analyzed.

A

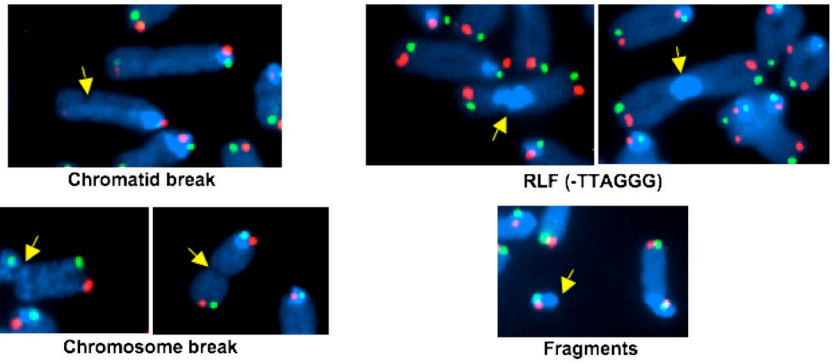

B

Frequency per metaphase	metaphase number	chromosome number	Fragments (+TTAGGG)	Fragments (-TTAGGG)	chromatid breaks	chromosome breaks	RLF (-TTAGGG)
Wild-type	91	7244	0.04 (4)	0.02 (2)	0.02 (2)	0.01 (1)	0.01 (1)
Suv4-20h1$^{-/-}$	42	3247	0.05 (2)	0.02 (1)	0	0.02 (1)	0.05 (2)
Suv4-20h2$^{-/-}$	63	4954	0	0	0	0.02 (1)	0.19 (12)
Suv4-20h dn	67	5530	0.03 (2)	0.06 (4)	0.07 (5)	0.01 (1)	0

Immunoprecipitated DNA was detected by Southern blotting with a telomeric probe (see ChIP section in Materials and methods). As shown in Fig. 3 (A and B), the loss of Suv4-20h1 HMTase does not lead to decreased H4K20me3 at telomeres. In contrast, Suv4-20h2$^{-/-}$ cells and, to a larger extent, Suv4-20h dn cells showed a marked decrease in H4K20me3 at telomeric chromatin compared with wild-type controls (*t* test; $P < 0.005$ for both comparisons; Fig. 3, A and B). These results were also confirmed using ES cells doubly deficient for Suv4-20h1 and h2 enzymes (Suv4-20h dn ES cells; Fig. 3, C and D). As a control, we also observed the loss of H4K20me3 at pericentric heterochromatin upon the abrogation of Suv4-20h2 or both Suv4-20h1 and h2 HMTases compared with wild-type controls (*t* test; $P < 0.05$ for both comparisons; Fig. 3, A and B; Schotta et al., 2004). Trimethylation of H3K9 was not substantially altered at telomeric and pericentric heterochromatin by the loss of Suv4-20h HMTases (Fig. 3, A–D), which is in agreement with a previous study showing a normal trimethylation of H3K9 in the presence of H4K20 trimethylation defects (Gonzalo et al., 2005). Indeed, it has been previously proposed that the assembly of telomeric and pericentric heterochromatin occurs sequentially and that trimethylation of H4K20 requires previous H3K9me3 by the Suv39h HMTases and not vice versa (Schotta et al., 2004; Gonzalo et al., 2005).

We next evaluated whether Suv4-20h deficiency affected the binding density of telomere repeat–binding factors TRF1 and TRF2 to telomeres, which were previously shown to have an important role in telomere length regulation (for review see de Lange, 2005). ChIP did not reveal any significant differences in the binding density of TRF1 or TRF2 to telomeric chromatin in the different Suv4-20 genotypes when using either MEF or ES cells ($P \geq 0.04$ for all comparisons; *t* test; Fig. 3, E and F). These results suggest that Suv4-20h deficiency does not dramatically alter the binding density of TRF1 and TRF2 to telomeric chromatin, although we cannot rule out that altered expression of other telomere-binding factors (for review see de Lange, 2005) as the consequence of Suv4-20h ablation could contribute to the long-telomere phenotype of these cells.

Abrogation of Suv4-20h HMTases results in decreased H4K20me3 at subtelomeric chromatin

We next evaluated whether the adjacent subtelomeric regions, which were recently characterized as chromatin domains enriched in H4K20me3 and H3K9me3 heterochromatic marks (Gonzalo et al., 2006), were affected by abrogation of the Suv4-20h HMTases. To this end, we performed ChIP assays followed by real-time PCR to detect these modifications at two independent subtelomeric regions in chromosomes 1 and 2 (Fig. 4, A and B; see Real-time quantitative PCR section in Materials and methods; Benetti et al., 2007). After normalization of the ChIP signals to the different inputs, we found no decrease in the levels of H3K9 trimethylation at these subtelomeric regions in the different Suv4-20h–deficient MEFs; instead, this modification was slightly increased in Suv4-20h dn MEFs compared with wild-type controls ($P < 0.05$ for both subtelomeric regions; Fig. 4, A and B). In contrast, H4K20 trimethylation was significantly decreased at chromosome 1 and 2 subtelomeric regions in Suv4-20h2–deficient cells (*t* test; $P \leq 0.05$; Fig. 4, A and B), and this reduction was further aggravated in cells deficient for both Suv4-20h1 and h2 HMTases (*t* test; $P < 0.01$; Fig. 4, A and B). Similar to that previously shown for telomeric chromatin, Suv4-20h1$^{-/-}$ cells did not show decreased H4K20me3 at subtelomeric chromatin domains (Fig. 4, A and B), indicating that the Suv4-20h2 HMTase is the one responsible for this histone modification at both telomeric and subtelomeric chromatin.

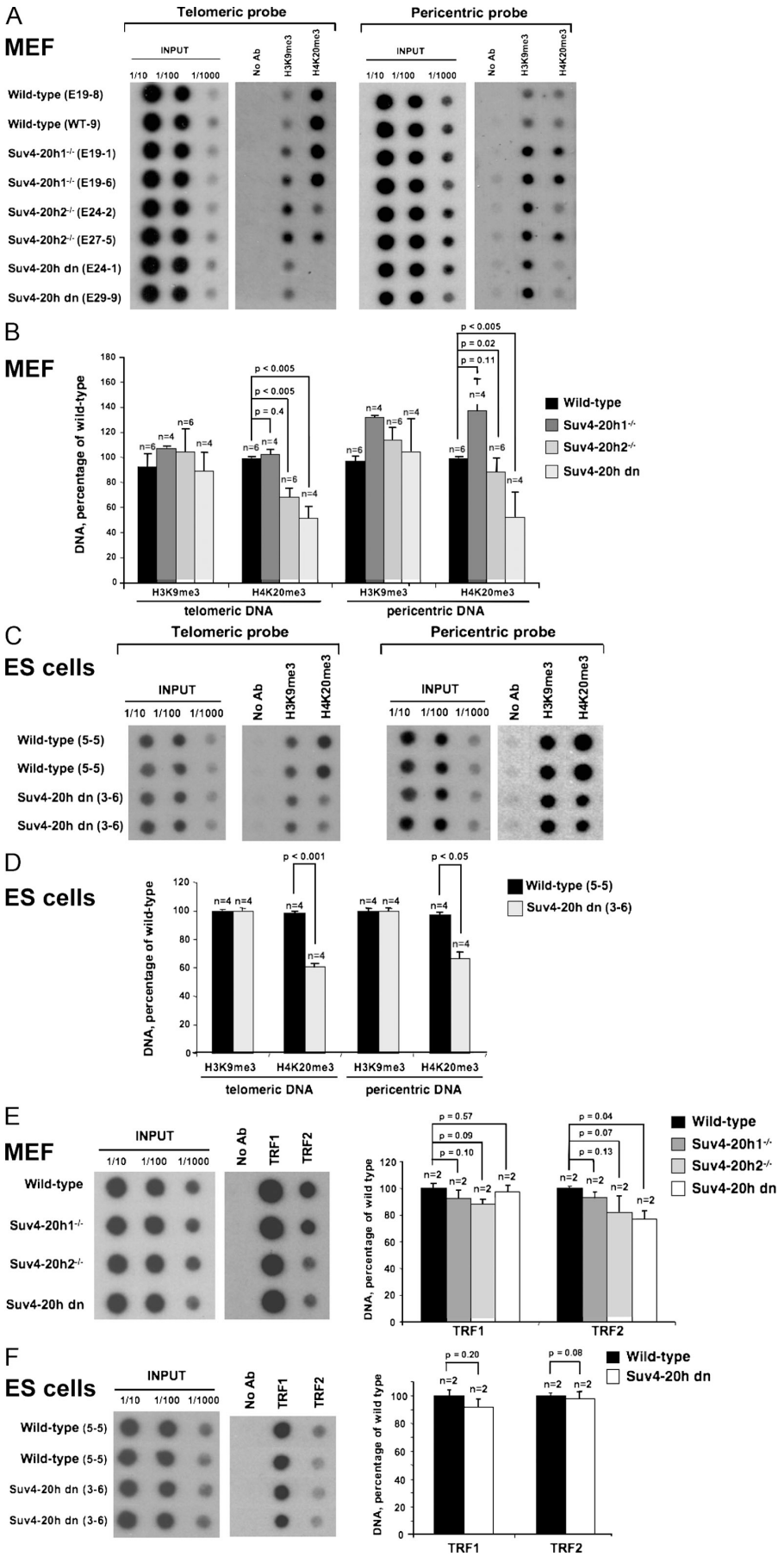

Figure 3. **Defective assembly of telomeric chromatin in Suv4-20h–deficient MEFs.** (A and B) ChIP of wild-type, Suv4-20h1$^{-/-}$, Suv4-20h2$^{-/-}$, and Suv4-20h dn MEFs with the indicated antibodies. Quantification of immunoprecipitated telomeric and pericentric repeats was normalized to input signals. Numbers in parentheses refer to individual MEF cultures. (B) At least two independent cultures per genotype were used for the analysis. No reproducible changes in H3K9me3 at telomeres or pericentric chromatin were observed between WT and the different Suv4-20h–deficient cells. In contrast, H4K20me3 was significantly reduced both at telomeric and pericentric heterochromatin in Suv4-20h2$^{-/-}$ and Suv4-20h dn MEFs but not in Suv4-20h1$^{-/-}$ MEFs. (C and D) ChIP of wild-type and Suv4-20h dn ES cells with the indicated antibodies. Quantification of immunoprecipitated telomeric and pericentric repeats was normalized to input signals. Numbers in parentheses refer to individual ES cell cultures. (D) No reproducible changes in H3K9me3 at telomeres or pericentric chromatin were observed between WT and Suv4-20h dn cells. In contrast, H4K20me3 was significantly reduced both at telomeric and pericentric heterochromatin in Suv4-20h dn ES cells. (E) ChIP of wild-type, Suv4-20h1$^{-/-}$, Suv4-20h2$^{-/-}$, and Suv4-20h dn MEFs with TRF1 and TRF2 antibodies. Quantification of immunoprecipitated telomeric repeats was normalized to input signals. (F) ChIP of wild-type and Suv4-20h dn ES cells with TRF1 and TRF2 antibodies. Quantification of immunoprecipitated telomeric repeats was normalized to input signals. (B, and D–F) ChIP values are represented as percentages of the wild-type, which was set to 100. (B and D–F) Error bars correspond to SD of the total number of ChIP assays performed for each genotype (*n*).

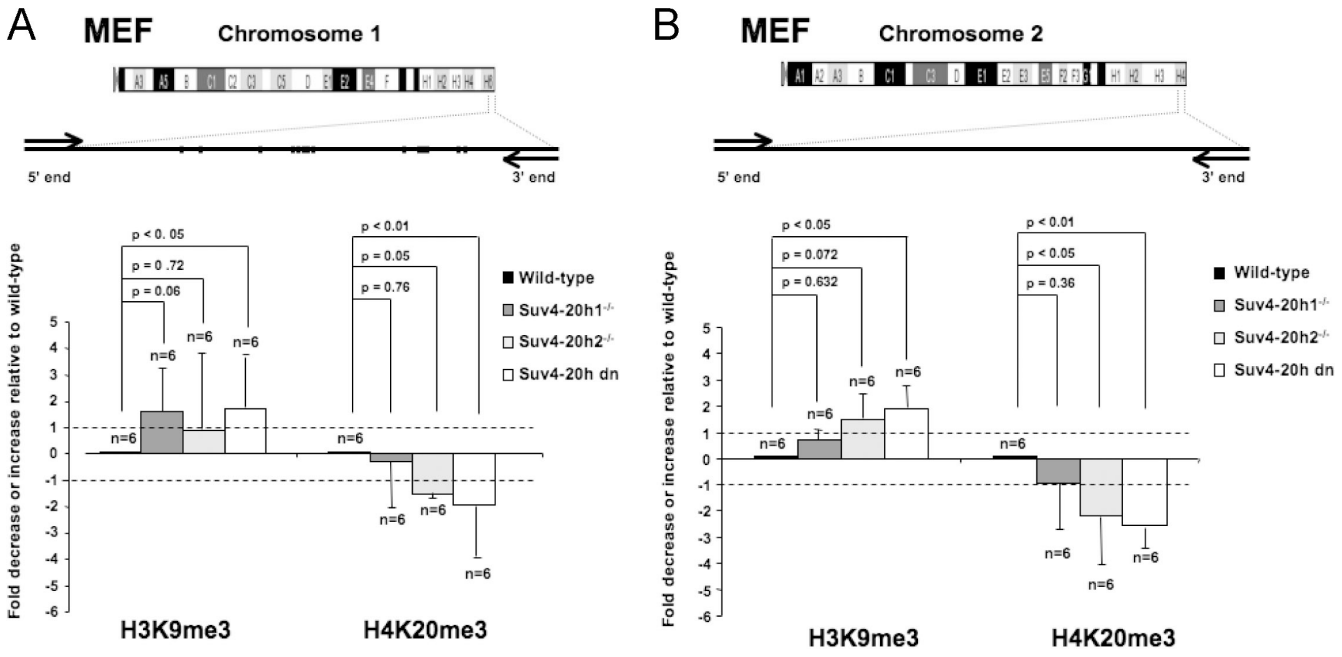

Figure 4. **Defective assembly of subtelomeric chromatin in Suv4-20h–deficient MEFs.** (A) Scheme of chromosome 1 used for RT-PCR analysis of subtelomeric histone modifications. RT-PCR–based ChIP analysis of H3K9me3 and H4K20me3 abundance is quantified in the bottom panel. At least two independent MEF cultures per genotype were used for the analysis. (B) Scheme of chromosome 2 used for RT-PCR analysis of subtelomeric histone modifications. RT-PCR–based ChIP analysis of H3K9me3 and H4K20me3 abundance is quantified in the bottom panel. At least two independent MEF cultures per genotype were used for the analysis. (A and B) Primer sequences are shown in Materials and methods. Error bars represent SD of the total number of ChIP assays performed for each genotype (*n*).

As a control, we confirmed the lack of these epigenetic modifications in a region of the p16 promoter known to be transcriptionally active and devoid of these heterochromatic marks (Gonzalo et al., 2006; unpublished data). Finally, these results were confirmed using Suv4-20h dn ES cells, which also showed a significant decrease ($P < 0.01$) in H4K20 trimethylation at both chromosome 1 and 2 subtelomeric regions in the absence of changes in H3K9 trimethylation (Fig. S1, available at http://www.jcb.org/cgi/content/full/jcb.200703081/DC1).

We have recently found that subtelomeric regions are also enriched in methylated CpG residues, which are maintained by the Dnmt1 and Dnmt3a,3b DNA methyltransferases (Gonzalo et al., 2006), further supporting the idea that subtelomeric regions are heterochromatic. To asses whether the loss of H4K20 trimethylation at subtelomeres in Suv4-20h–deficient cells resulted in decreased DNA methylation at these regions, we determined the percentage of CpG residues that are methylated at the subtelomeric regions in the chromosomes 1 and 2 described above in this same section (Fig. 5, A and B) and that were previously shown by us to be heavily methylated (Benetti et al., 2007). To this end, we used bisulfite sequencing of CpG residues (see Analysis of genomic subtelomeric DNA methylation section in Materials and methods). As expected, we found that both chromosome 1 and 2 subtelomeric regions were heavily methylated in wild-type MEFs (Fig. 5, A and B). However, abrogation of either the Suv4-20h1 or h2 enzyme did not result in the significantly decreased DNA methylation of these regions (Fig. 5, A and B) except for a slight decrease in the frequency of methylated CpG residues in Suv4-20h dn MEFs at the subtelomeric region of chromosome 2 (χ^2 test; $P < 0.005$; Fig. 5 B), which was not observed at the subtelomeric region of chromosome 1 (χ^2 test; $P = 0.09$; Fig. 5 A). To confirm these results, we also studied subtelomeric DNA methylation in ES cells deficient for the Suv39h1 and h2 HMTases (Suv39h dn cells), which were previously shown to be upstream of the Suv420h HMTases and, therefore, are required for H4K20 trimethylation at heterochromatic domains (Schotta et al., 2004). As shown in Fig. S2 (available at http://www.jcb.org/cgi/content/full/jcb.200703081/DC1), we observed a normal or even increased DNA methylation at chromosome 1 and 2 subtelomeric regions in Suv39h dn ES cells compared with the wild-type controls. Altogether, these results demonstrate that Suv4-20h2 is largely responsible for the trimethylation of H4K20 at both telomeric and subtelomeric heterochromatin domains but that this modification does not seem to impinge on subtelomeric DNA methylation.

Increased telomere recombination events in cells defective in telomeric heterochromatin histone methylation marks

We have previously shown that loss of DNA methylation results in increased recombination between telomeric sequences, as indicated by an elevated number of T-SCEs in cells lacking the Dnmt1 and Dnmt3a,3b DNA methyltransferase activities (Gonzalo et al., 2006). This increased recombination among telomeric sequences has been described to be correlative with activation of the ALT pathway for telomere length maintenance (Bailey et al., 2004; Bechter et al., 2004), although evidence for a causal relationship between both processes is still pending.

With this idea in mind, we hypothesized that other epigenetic alterations that may affect the structure of the telomeric or

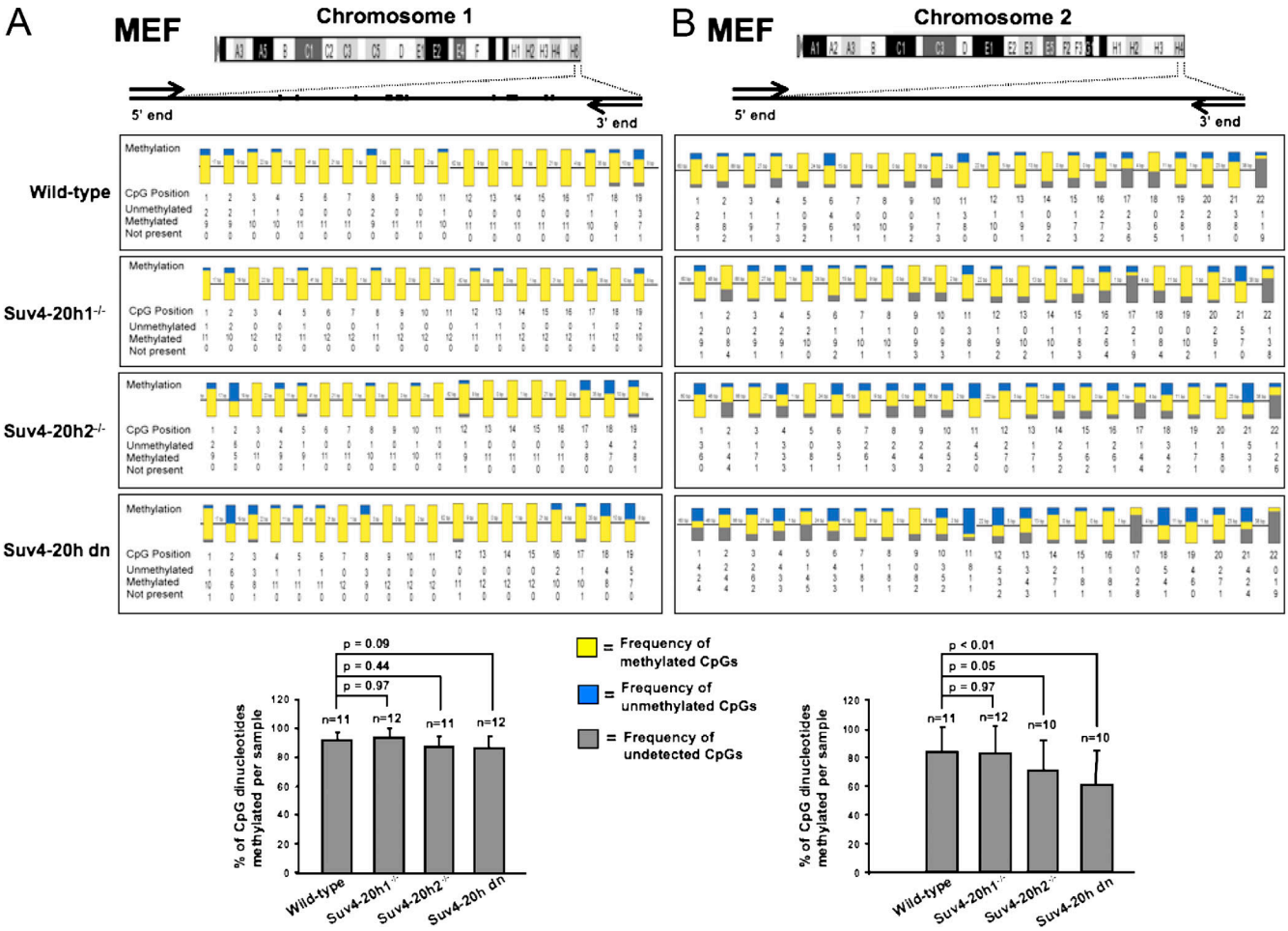

Figure 5. **Normal DNA methylation of subtelomeric domains in Suv4-20h–deficient MEFs.** (A) Scheme of chromosome 1 depicting the subtelomeric region used for bisulfite genomic sequencing. 11–12 independent clones per genotype were analyzed (*n*). Yellow and blue represent the frequency of methylated and unmethylated CpG dinucleotides, respectively, at each position. Quantification of the percentage of methylated CpGs per sample after bisulfite genomic sequencing of 11–12 clones of each genotype is shown in the bottom panel. (B) Scheme of chromosome 2 depicting the subtelomeric region used for bisulfite genomic sequencing. 10–12 independent clones per genotype were analyzed (*n*). Yellow and blue represent the frequency of methylated and unmethylated CpG dinucleotides, respectively, at each position. Quantification of the percentage of methylated CpGs per sample after bisulfite genomic sequencing of 10–12 clones of each genotype is shown in the bottom panel. (A and B) Error bars represent SD of the differences among all independent clones (*n*). Primer sequences are provided in Materials and methods.

subtelomeric chromatin, such as defects in histone methylation, could also have an impact on the rate of recombination among telomeric sequences. To test this hypothesis, we determined the frequency of T-SCE events in cells that lack the Suv39h and Suv4-20h HMTase activities, which have been shown to have defects in telomere chromatin assembly and telomere length maintenance (Garcia-Cao et al., 2004; this study). To this end, we used the two-color chromosome orientation FISH or chromosome orientation FISH technique, which allows us to detect SCE events specifically at telomere repeats (see Chromosome orientation FISH section in Materials and methods; Bailey et al., 2004; Bechter et al., 2004; Gonzalo et al., 2006). Notably, we considered it a positive T-SCE event only when it was simultaneously detected at both the leading and lagging strand telomere as an unequal exchange of telomeric signal (see representative examples in Fig. 6, A–C; yellow arrows). We first analyzed MEFs lacking the Suv4-20h1 and h2 HMTases (Suv4-20h1$^{-/-}$, Suv4-20h2$^{-/-}$, and Suv4-20h dn MEFs). Suv4-20h2$^{-/-}$ and Suv4-20h dn MEFs showed a significant increase in the frequency of T-SCE events compared with the wild-type controls (χ^2 test; $P < 0.05$ for both comparisons; Fig. 6 A). In contrast, Suv4-20h1$^{-/-}$ MEFs showed a slightly decreased frequency of T-SCE events than wild-type cells, although this difference did not reach statistical significance (χ^2 test; $P = 0.3271$; Fig. 6 A). Notably, both Suv4-20h2$^{-/-}$ and Suv4-20h dn MEFs showed an increased telomere length compared with wild-type controls, whereas Suv4-20h1$^{-/-}$ showed slightly shorter telomeres (Fig. 1), suggesting a correlation between telomere elongation and an increase in T-SCE in these genotypes.

Next, we evaluated whether ES cells lacking either the Suv4-20h or Suv39h HMTases also presented deregulated telomeric recombination. We detected a significant increase in the frequency of T-SCE events per chromosome in both Suv4-20h dn and Suv39h dn ES cells (χ^2 test; $P < 0.0001$ for both cases; Fig. 6, B and C), although the phenotype was more severe in the Suv39h dn ES cells. Notably, the frequencies of T-SCE in ES

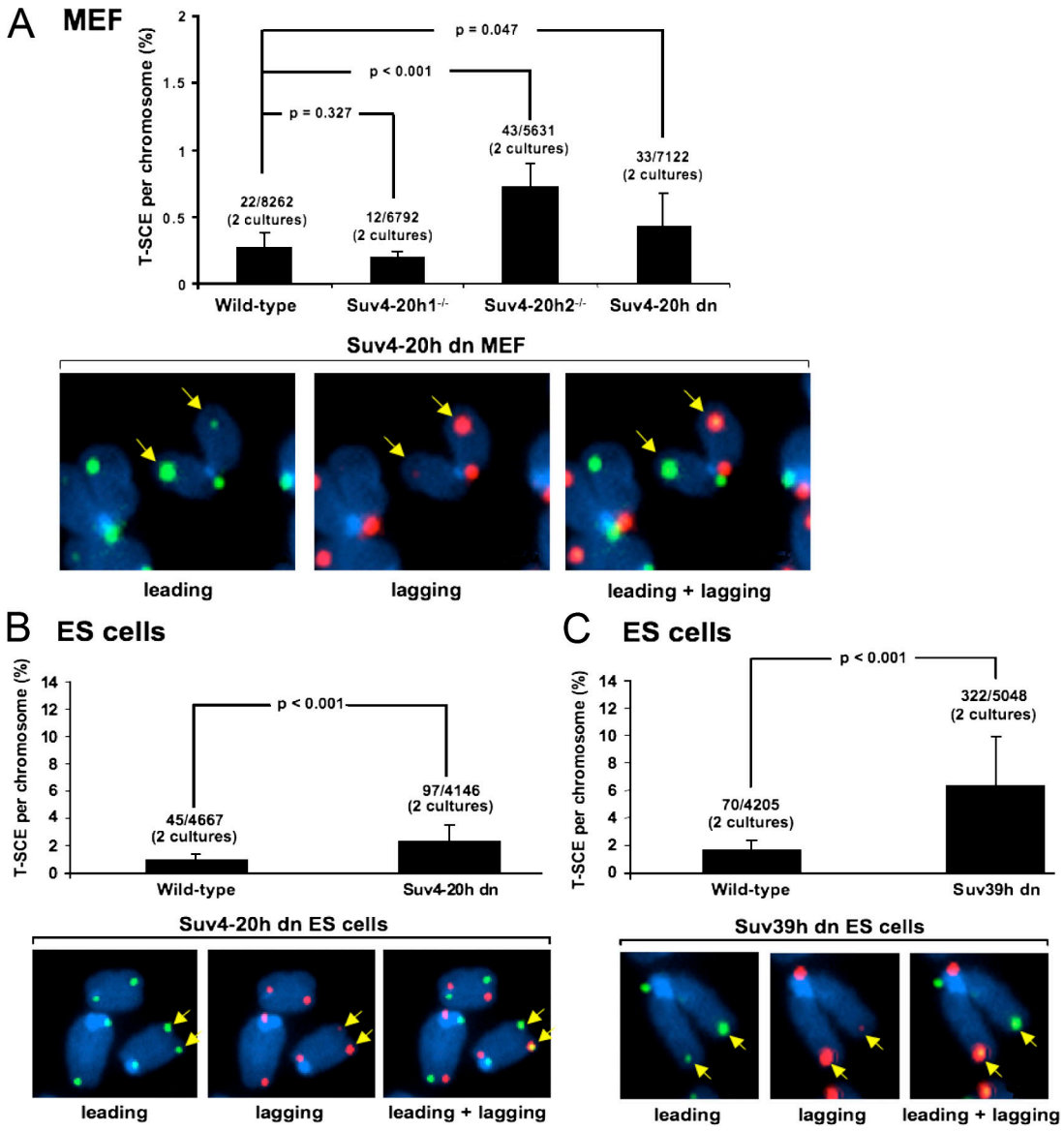

Figure 6 . **Increased telomeric SCE in cells deficient for HMTases Suv39h and Suv4-20h.** (A) Quantification of T-SCE events in wild-type and the indicated Suv4-20h–deficient cells. A significant increase in T-SCE is observed in Suv4-20h2$^{-/-}$ and Suv4-20h dn MEFs (χ^2 test; $P < 0.05$) but not in Suv4-20h1$^{-/-}$ MEFs (χ^2 test; $P = 0.3271$). The total number of T-SCE events out of the total number of chromosomes analyzed (between 5,000 and 8,000) is indicated on top of each bar. Error bars correspond to SD of the total number of independent MEF cultures used for the analysis (*n*). (B) Quantification of T-SCE events in wild-type and Suv4-20h1/h2–deficient ES cells (Suv39h dn ES cells). A significant increase in T-SCE is observed in Suv4-20h dn ES cells compared with the wild-type controls (χ^2 test; $P < 0.0001$). The total number of T-SCE events out of the total number of chromosomes analyzed (>4,000) is indicated on top of each bar. Error bars correspond to SD of the total number of independent ES cultures used for the analysis (*n*). (C) Quantification of T-SCE events in wild-type and Suv39h1/h2-deficient cells (Suv39h dn cells). A significant increase in T-SCE is observed in Suv39h dn ES cells compared with the wild-type controls (χ^2 test; $P < 0.0001$). The total number of T-SCE events out of the total number of chromosomes analyzed (between 4,000 and 5,000) is indicated on top of each bar. Error bars correspond to the total number of independent ES cultures used for the analysis (*n*). (A–C) Representative chromosome orientation FISH images after labeling leading (green) and lagging (red) strand telomeres are shown in the bottom panel. The yellow arrows indicate chromosomes showing recombination between telomeres. Note that in all cases, a T-SCE event was only considered positive when it was observed both at the lagging and leading strand telomeres as an unequal exchange of telomeric signal.

cells were higher than in MEFs (compare T-SCE frequencies in wild-type and Suv4-20h dn MEFs with ES cells in Fig. 6, A and B), which is in agreement with a previous study's finding that telomeres in ES cells are more recombinogenic than those of other cell types (Wang et al., 2005). Importantly, these results suggest that not only DNA methyltransferases but also other chromatin-modifying activities such as the Suv4-20h and Suv39h dn HMTases are necessary to prevent sister chromatid recombination events between the highly repetitive telomeric sequences. Indeed, Suv39h dn ES cells showed similarly elevated T-SCE frequencies to those previously described for Dnmt-deficient ES cells (Gonzalo et al., 2006). To address whether Suv4-20h and Suv39h deficiencies also resulted in increased sister chromatid recombination throughout the genome, we determined the frequency of global SCE events in both MEFs and ES cells dn for either the Suv4-20h (Suv4-20h dn) or Suv39h enzymes (Suv39h dn).

As shown in Fig. S3 (A–C; available at http://www.jcb.org/cgi/content/full/jcb.200703081/DC1), both MEF and ES cells deficient for either the Suv4-20h or Suv39h enzymes showed a significantly elevated frequency of SCE compared with the corresponding wild-type controls (χ^2 test; $P < 0.005$ for all cases), suggesting that the global loss of H3K9me3 and H4K20me3 results in increased frequencies of recombination between sister chromatids.

To further address whether Suv4-20h dn and Suv39h dn ES cells showed an increased activation of ALT pathways, we determined the presence of the so-called ALT-associated promyelocytic leukaemia (PML) bodies or ALT-associated PML bodies (APBs), which, together with increased T-SCE, also correlate with activation of the ALT pathway (Muntoni and Reddel, 2005; Gonzalo et al., 2006). This is characterized by the colocalization of telomeres and the PML protein (Fig. 7, A and B; arrowheads). Suv4-20h dn ES cells showed a significant increase in the frequency of cells showing APBs, which represented a 1.4-fold increase compared with wild-type controls (χ^2 test; $P < 0.0014$; Fig. 7 A). Suv39h dn ES cells showed a further increase in the frequency of cells showing APBs, which represented a 2.3-fold increase compared with wild-type controls (χ^2 test; $P < 0.0001$; Fig. 7 B). These findings agree with the increased T-SCE frequencies of both Suv4-20h dn and Suv39h dn ES cells and suggest the activation of ALT pathways associated with defective histone methylation at telomeres and subtelomeres.

Discussion

Recent studies have stressed the importance of the acquisition of a specific chromatin structure at telomeres to maintain telomere length homeostasis in mammals (Blasco, 2005; for review see de Lange, 2005). In addition, the architecture of the adjacent subtelomeric chromatin has also been proven to be critical for telomere length control (Gonzalo et al., 2006). In this study, we have identified the Suv4-20h HMTases as active regulators of the assembly of telomeric and subtelomeric chromatin by undertaking the trimethylation of H4K20 at these domains. Importantly, the loss of Suv4-20h2 activity or simultaneous abrogation of Suv4-20h1/h2 activities and, consequently, of the H4K20me3 mark lead to telomere length deregulation. These results support the notion that epigenetic alterations consisting of the loss of repressive chromatin-modifying activities lead to telomere elongation. It is interesting to note that Suv4-20h1 deficiency did not result in decreased H4K20 trimethylation at either telomeric or pericentric chromatin, suggesting that Suv4-20h2 is the main enzyme responsible for this histone modification at heterochromatic domains. Similarly, Suv4-20h1 deficiency did not result in increased telomere length or increased T-SCE frequencies, suggesting a direct correlation between the loss of H4K20 trimethylation at telomeres and the occurrence of these telomere phenotypes. It is also important to highlight that Suv4-20h deficiency is likely to have global effects in sister chromatid recombination that are not just restricted to the telomeric regions, as indicated by elevated SCE events in Suv4-20d dn MEF and ES cells compared with the wild-type controls.

Altogether, these results suggest a model in which the opening of telomeric chromatin by the loss of repressive chromatin marks could facilitate the accessibility of telomerase or other telomere-elongating activities to the telomere, leading to telomere elongation. Two main mechanisms have been described for the maintenance of mammalian telomeres: the addition of telomeric repeats by telomerase and an alternative mechanism (ALT) that relies on the recombination between telomeric sequences to maintain telomere length. So far, the accessibility of telomerase to telomeres in epigenetically altered mouse cells has not been evaluated. Regarding the derepression of ALT, we have previously demonstrated that DNA hypomethylation results in a marked increase in recombination among telomeric sequences concomitant with aberrant telomere elongation (Gonzalo et al., 2006). In the present study, we demonstrate that abrogation of either Suv39h, Suv4-20h2, or both Suv4-20h1/h2 HMTase activities also leads to elongated telomeres and increased recombination between telomeric repeats in the absence of major DNA methylation defects at subtelomeric regions. This is in contrast to previous results showing that cells lacking Suv39h HMTases also present defects in DNA methylation at pericentric repeats (Lehnertz et al., 2003). Therefore, our results suggest that the increased recombination among telomeric sequences described here for both Suv4-20h and Suv39h-deficient cells is associated with the loss of H4K20me3 and H3K9me3 histone marks and is independent of subtelomeric DNA methylation (see model in Fig. S4 and see Table S1 for a summary of the data; available at http://www.jcb.org/cgi/content/full/jcb.200703081/DC1). In agreement with this, Suv39h dn cells, which have decreased levels of both H4K20me3 and H3K9me3 marks, show more severe phenotypes in T-SCE and APB frequencies than Suv4-20h dn cells.

Finally, the results described here support the previously proposed sequential model of chromatin assembly at mouse pericentric heterochromatin (Schotta et al., 2004) in which the Suv4-20h HMTases act downstream of the Suv39h HMTases (see model in Fig. S4). Altogether, our results demonstrate that the proper action of HMTases inhibits random recombination events and also ensures telomere length homeostasis. These findings are potentially important for cancer research because studies have shown that tumor cells undergo a series of epigenetic modifications, such as global DNA hypomethylation, and a global decrease in H4K20 trimethylation and H4K16 acetylation (Jones and Baylin, 2002; Fraga et al., 2005). One can envision that in tumor cells that present these epigenetic defects, telomere length maintenance may be favored, with the consequent growth advantage that this will provide to the tumor cells.

Materials and methods

Cell culture

MEFs were prepared from wild-type, Suv4-20h1$^{-/-}$, Suv4-20h2$^{-/-}$, and Suv4-20h1/h2 dn (Suv4-20h dn) embryos. Wild-type and Suv4-20h1/h2 dn ES cells were also generated. MEF cells and ES cells from wild type and Suv39h dn were previously described (Peters et al., 2001).

TRF analysis

Cells were included in agarose plugs, and TRF analysis was performed as previously described (Blasco et al., 1997).

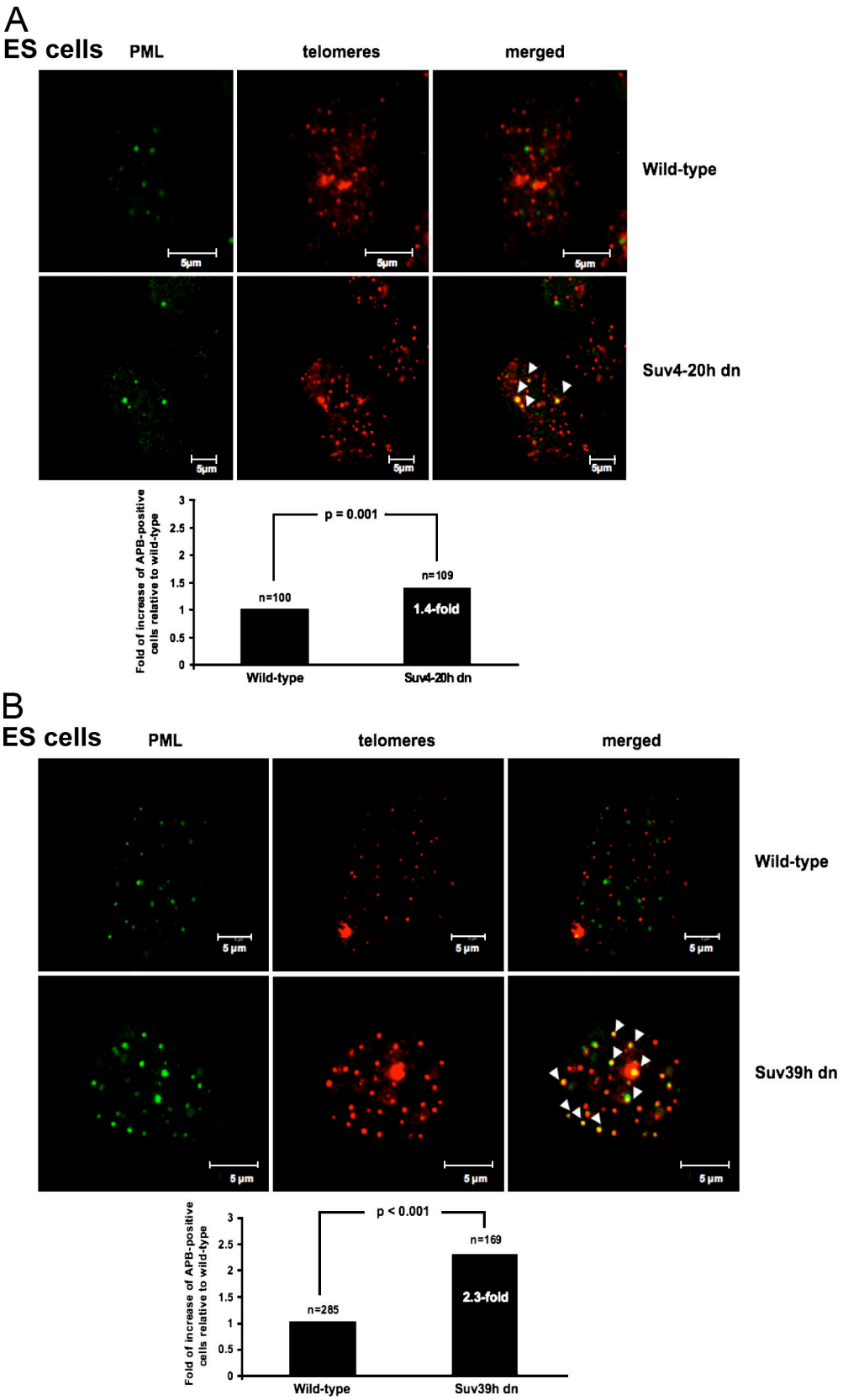

Figure 7 . **Increased APBs in ES cells deficient for Suv4-20h and Suv39h HMTases.** (A and B) Confocal microscopy images showing either PML fluorescence (green), telomere fluorescence (red), or combined fluorescence (yellow) in wild-type, Suv4-20h dn (A), and Suv39h dn (B) ES cells. Note that some of the PML bodies in HMT-deficient cells colocalize with telomeric DNA (indicated by arrowheads), and this is not seen in wild-type cells. Fold increase of the percentage of cells showing the colocalization of telomeres with PML protein is shown in the bottom panels. A cell was considered positive when it showed two or more colocalization events. An increased frequency of cells showing APBs is observed in the Suv4-20h dn and Suv39h dn ES cells when compared with the WT ES cells. The total number of cells used for the analysis is indicated (*n*).

Bal31 digestions

Before digestion with MboI (Blasco at al., 1997), agarose plugs were digested with 3 U Bal31 exonuclease (New England Biolabs, Inc.) at 30°C during 90 min after 1-h preincubation in Bal31 buffer.

Q-FISH analysis

We prepared metaphases and performed Q-FISH hybridization as previously described (Herrera et al., 1999; Samper et al., 2000). To correct for lamp intensity and alignment, we analyzed images from fluorescent beads (Invitrogen) using the TFL-Telo program (gift from P. Lansdorp, Terry Fox Laboratory, British Columbia Cancer Research Centre, Vancouver, Canada). Telomere fluorescence values were extrapolated from the telomere fluorescence of lymphoma cell lines LY-R (R cells) and LY-S (S cells) with known telomere lengths of 80 kb and 10 kb, respectively. There was a linear correlation ($r2 = 0.999$) between the fluorescence intensity of the R and S telomeres. We recorded the images using a CCD camera (FK7512; COHU) on a fluorescence microscope (DMRB; Leica). A mercury vapor lamp (CS 100 W-2; Philips) was used as a source. We captured the images using Q-FISH software (Leica) in a linear acquisition mode to prevent the oversaturation of fluorescence intensity. We used the TFL-Telo software (Zijlmans et al., 1997) to quantify the fluorescence intensity of telomeres from at least five metaphases for each data point.

ChIP

ChIP assays were performed as previously described (Garcia-Cao et al., 2004). In brief, after cross-linking and sonication, 3×10^6 cells (MEFs or ES cells) were used per immunoprecipitation with anti-H3K9me3 or anti-H4K20me3 antibodies (Upstate Biotechnology) or anti-TRF1 raised in our laboratory against full-length mouse TRF1 and anti-TRF2 (provided by E. Gilson, Ecole Normale Superieure de Lyon, Lyon, France). The immunoprecipitated DNA was transferred to a nitrocellulose membrane using a dot blot apparatus. The membrane was then hybridized with either a telomeric probe or a probe recognizing major satellite sequences, which is characteristic of pericentric heterochromatin. Quantification of the signal was performed with ImageQuant software (Molecular Dynamics). The amount of telomeric and pericentric DNA after ChIP was normalized to the total input signal for each genotype.

Real-time quantitative PCR for the detection of subtelomeric histone modifications

The presence of subtelomeric sequences of chromosomes 1 and 2 in ChIP samples was detected using primers Chr1-bis-end-5′ (TTAGGACTTCTGGCTTCGGTAG) and Chr1-bis-end-3′ (AGCTGTGGCAGGCATCGTGGC) for chromosome 1 and Chr2-tris-end-5′ (GAATCCTCCCTGTAGCAGGG) and Chr2-tris-end-3′ (GTACATAACCGATCCAGGTGTG) for chromosome 2. We performed real-time quantitative PCR and calculated the $\Delta\Delta C_t$ value, which represents the cycle threshold difference between the subtelomeric primer pair and the input primer pair. In all cases, PCR was repeated at least five times. ChIP values were represented relative to those of wild-type cells.

Chromosome orientation FISH

Confluent MEF and ES cells were subcultured in the presence of BrdU (Sigma-Aldrich) at a final concentration of 1×10^{-5} M and were then allowed to replicate their DNA once at 37°C for 24 h and 12 h, respectively. Colcemid was added in a concentration of 0.2 μg/ml for MEFs and 1 μg/ml for ES cells for the last 4 h and 1 h, respectively. Cells were then recovered, and metaphases were prepared as described previously (Samper et al., 2000). Chromosome orientation FISH was performed as previously described (Bailey et al., 2001, Gonzalo et al., 2006) using first a $(CCCTAA)_7$ PNA probe labeled with Cy3 and then a second $(TTAGGG)_7$ PNA labeled with fluorescein (Applied Biosystems). Metaphase spreads were captured on a fluorescence microscope (DMRB; Leica).

Differential staining technique for SCE

Genomic SCEs were visualized using an adapted Fluorescence-Plus-Giemsa protocol (Perry and Wolff, 1974). In brief, confluent MEFs and ES cells were subcultured in the presence of BrdU (Sigma-Aldrich) at a final concentration of 1×10^{-5} M and were then allowed to replicate their DNA twice at 37°C for 48 h and 24 h, respectively. Colcemid was added in a concentration of 0.2 μg/ml for MEFs and 1 μg/ml for ES cells for the last 4 h and 1 h, respectively. Cells were then recovered, and metaphases were prepared as described for the Q-FISH (Samper et al., 2000). Slides were stained in 200 μg/ml Hoechst 33258 in water for 30 min at room temperature, rinsed with distilled H_2O, and allowed to air dry. Slides were then mounted with 2× SSC and exposed to UV light for 30 min. After being rinsed with distilled H_2O, slides were air dried. Finally, they were stained with Leishman's stain (Sigma-Aldrich) for 4 min. Metaphases were captured using brightfield microscopy (AX70; Olympus) and analyzed for harlequin staining. Each color switch was scored as one SCE.

Confocal immunofluorescence FISH experiments

For confocal immunostaining experiments, 50,000 cells (MEFs or ES cells) were seeded in multiwell immunofluorescence slides (LABTEK n°154534; Nunc). After 24 h in culture, cells were washed twice with 1× PBS and fixed for 20 min at 4°C in 4% PFA in 1× PBS. Cells were then washed twice with 1× PBS and treated with 0.1% Triton X-100 in 1× PBS at RT for 7 min followed by two washes with PBS. After blocking with 10% BSA (in PBS) at 37°C for 20 min, cells were incubated with rabbit anti–mouse PML polyclonal antibody (gift from P. Freemont, Cancer Research UK, London, UK) diluted 1:1,000 in blocking solution overnight at 4°C. After washing twice with 0.05% Triton X-100 in PBS for 5 min, cells were incubated with a secondary goat anti–rabbit IgG conjugated with AlexaFluor488 and diluted 1:300 in blocking solution for 1 h at RT. After immunostaining, telomeric FISH was performed as described previously (Samper et al., 2000) with minor modifications. In brief, slides were first washed twice with PBS and fixed for 2 min in 4% formaldehyde. After washing three times with PBS, slides were dehydrated in ethanol series (70, 90, and 100%) and air dried. Hybridization with Cy3-labeled telomeric PNA probe was performed as described for Q-FISH analysis. After hybridization, slides were washed twice with 50% formamide/10 mM Tris, pH 7.2/0.1% BSA for 15 min followed by three washes with 0.1 M Tris/0.15 M NaCl, pH 7.5/0.08% Tween 20 for 5 min. Slides were then dehydrated with ethanol series and air dried. Finally, slides were counterstained with 0.2 μg/ml DAPI in Vectashield (Vector Laboratories). Images were captured at room temperature in a confocal microscope (TCS SP2-A-OBS-UV; Leica) and analyzed by confocal software (Leica).

Analysis of genomic subtelomeric DNA methylation

The methylation status of the different subtelomeric genomic DNA regions was established by PCR analysis after bisulfite modification. Bisulfite genomic sequencing was performed as described previously (Fraga et al., 2005). Automatic sequencing of 7–14 colonies for each sequence was performed to obtain statistical data on the methylation status of every single subtelomeric CpG island. Bisulfite genomic sequencing primers were designed against subtelomeric regions in chromosome 1. The primer sequences used were CACCTCTAACCACTTAAACCTAACAA and GGGGTAGATATTTAGGGAAGG, which flank positions 197042227–197042569 of chromosome 1 in the mouse National Center for Biotechnology Information (NCBI) 36 genome assembly, and TTACCAATACCACCATTCCTCCA and GAGAGTAGTTAATTAGATGAGGAATA, which flank positions 181837807–181838281 at chromosome 2 in the mouse NCBI 36 genome assembly. Results were analyzed with the BiQ Analyzer program.

Statistical calculations

A Wilcoxon rank-sum test was used to calculate statistical significance differences for telomere length differences. A two-tailed *t* test was used to assess the statistical significance of the observed differences in ChIP and RT-PCR analyses. Prism (version 4; GraphPad) and Excell software (version 2003; Microsoft) were used for statistical calculations.

To calculate the statistical significance of differences in subtelomeric DNA methylation, SCE, T-SCE, and APB frequencies, we used the χ^2 test. The two-sided p-values presented were obtained from a 2×2 contingency table analyzed by the χ^2 test (including Yates' continuity correction). Instat (version 3.05; GraphPad) was used for the calculations. In all cases, differences are significant for $P < 0.05$, very significant for $P < 0.01$, highly significant for $P < 0.001$, and extremely significant for $P < 0.0001$.

Online supplemental material

Fig. S1 shows the defective assembly of subtelomeric chromatin in Suv4-20h–deficient ES cells. Fig. S2 shows normal DNA methylation of subtelomeric domains in Suv39h-deficient ES cells. Fig. S3 shows increased global SCE in cells deficient for HMTase Suv39h and Suv4-20h. Fig. S4 depicts a model for chromatin assembly at mammalian telomeres and subtelomeres. Table S1 provides a summary of the effects of Suv39h and Suv420h deletion on telomere length, telomere recombination, and telomere structure. Online supplemental material is available at http://www.jcb.org/cgi/content/full/jcb.200703081/DC1.

We are indebted to the Genomics and Epigenomics Unit at the Spanish National Cancer Centre for bisulfite sequencing.

Research at the laboratory of T. Jenuwein is supported by the Research Institute of Molecular Pathology through Boehringer Ingelheim and by grants from the European Union (FP6 NoE-network The Epigenome) and the Genome Research in Austria initiative, which is financed by the Austrian Ministry of Education, Science, and Culture. G. Schotta is supported by a Marie Curie Intra-European Fellowship. M.A. Blasco's laboratory is funded by the Spanish Ministry of Education and Culture (grants SAF2001-1869 and GEN2001-4856-C13-08), Regional Government of Madrid (grant 08.1/0054/01), the European Union (grants TELOSENS FIGH-CT-2002-00217, INTACT LSHC-CT-2003-506803, ZINCAGE FOOD-CT-2003-506850, and RISC-RAD FI6R-CT-2003-508842), and the Josef Steiner Award 2003.

Submitted: 13 March 2007
Accepted: 9 August 2007

References

Bailey, S.M., M.N. Cornforth, A. Kurimasa, D.J. Chen, and E.H. Goodwin. 2001. Strand-specific postreplicative processing of mammalian telomeres. *Science*. 293:2462–2465.

Bailey, S.M., M.A. Brenneman, and E.H. Goodwin. 2004. Frequent recombination in telomeric DNA may extend the proliferative life of telomerase-negative cells. *Nucleic Acids Res.* 32:3743–3751.

Bechter, O.E., Y. Zou, W. Walker, W.E. Wright, and J.W. Shay. 2004. Telomeric recombination in mismatch repair deficient human colon cancer cells after telomerase inhibition. *Cancer Res.* 64:3444–3451.

Benetti, R., M. García-Cao, and M.A. Blasco. 2007. Telomere length regulates the epigenetic status of mammalian telomeres and subtelomeres. *Nat. Genet.* 39:243–250.

Blasco, M.A. 2005. Telomeres and human disease: ageing, cancer and beyond. *Nat. Rev. Genet.* 6:611–622.

Blasco, M.A. 2007. The epigenetic regulation of mammalian telomeres. *Nat. Rev. Genet.* 8:299–309.

Blasco, M.A., H.W. Lee, M.P. Hande, E. Samper, P.M. Lansdorp, R.A. DePinho, and C.W. Greider. 1997. Telomere shortening and tumor formation by mouse cells lacking telomerase RNA. *Cell*. 91:25–34.

Chan, S.W., and E.H. Blackburn. 2002. New ways not to make ends meet: telomerase, DNA damage proteins and heterochromatin. *Oncogene*. 21:553–563.

de Lange, T. 2005. Shelterin:the protein complex that shapes and safeguards human telomeres. *Genes Dev.* 19:2100–2110.

Dunham, M.A., A.A. Neumann, C.L. Fasching, and R.R. Reddel. 2000. Telomere maintenance by recombination in human cells. *Nat. Genet.* 26:447–450.

Fraga, M.F., E. Ballestar, A. Villar-Garea, M. Boix-Chornet, J. Espada, G. Schotta, T. Bonaldi, C. Haydon, S. Ropero, K. Petrie, et al. 2005. Loss of acetylation at Lys16 and trimethylation at Lys20 of histone H4 is a common hallmark of human cancer. *Nat. Genet.* 37:391–400.

Garcia-Cao, M., S. Gonzalo, D. Dean, and M.A. Blasco. 2002. A role for the Rb family of proteins in controlling telomere length. *Nat. Genet.* 32:415–419.

Garcia-Cao, M., R. O'Sullivan, A.H. Peters, T. Jenuwein, and M.A. Blasco. 2004. Epigenetic regulation of telomere length in mammalian cells by the Suv39h1 and Suv39h2 histone methyltransferases. *Nat. Genet.* 36:94–99.

Gonzalo, S., M. Garcia-Cao, M.F. Fraga, G. Schotta, A.H. Peters, S.E. Cotter, R. Eguia, D.C. Dean, M. Esteller, T. Jenuwein, and M.A. Blasco. 2005. Role of the RB1 family in stabilizing histone methylation at constitutive heterochromatin. *Nat. Cell Biol.* 7:420–428.

Gonzalo, S., I. Jaco, M.F. Fraga, T. Chen, E. Li, M. Esteller, and M.A. Blasco. 2006. DNA methyltransferases control telomere length and telomere recombination in mammalian cells. *Nat. Cell Biol.* 8:416–424.

Herrera, E., E. Samper, J. Martin-Caballero, J.M. Flores, H.W. Lee, and M.A. Blasco. 1999. Disease states associated with telomerase deficiency appear earlier in mice with short telomeres. *EMBO J.* 18:2950–2960.

Jones, P.A., and S.B. Baylin. 2002. The fundamental role of epigenetic events in cancer. *Nat. Rev. Genet.* 3:415–428.

Kourmouli, N., P. Jeppesen, S. Mahadevhaiah, P. Burgoyne, R. Wu, D.M. Gilbert, S. Bongiorni, G. Prantera, L. Fanti, S. Pimpinelli, et al. 2004. Heterochromatin and tri-methylated lysine 20 of histone H4 in animals. *J. Cell Sci.* 117:2491–2501.

Lachner, M., D. O'Carroll, S. Rea, K. Mechtler, and T. Jenuwein. 2001. Methylation of histone H3 lysine 9 creates a binding site for HP1 proteins. *Nature*. 410:116–120.

Lehnertz, B., Y. Ueda, A.A. Derijck, U. Braunschweig, L. Perez-Burgos, S. Kubicek, T. Chen, E. Li, T. Jenuwein, and A.H. Peters. 2003. Suv39h-mediated histone H3 lysine 9 methylation directs DNA methylation to major satellite repeats at pericentric heterochromatin. *Curr. Biol.* 13:1192–1200.

Muntoni, A., and R.R. Reddel. 2005. The first molecular details of ALT in human tumor cells. *Hum. Mol. Genet.* 14:R191–R196.

Perry, P., and S. Wolff. 1974. New Giemsa method for the differential staining of sister chromatids. *Nature*. 251:156–158.

Peters, A.H., D. O'Carroll, H. Scherthan, K. Mechtler, S. Sauer, C. Schöfer, K. Weipoltshammer, M. Pagani, M. Lachner, A. Kohlmaier, et al. 2001. Loss of the Suv39h histone methyltransferases impairs mammalian heterochromatin and genome stability. *Cell*. 107:323–337.

Samper, E., F.A. Goytisolo, P. Slijepcevic, P.P. van Buul, and M.A. Blasco. 2000. Mammalian Ku86 protein prevents telomeric fusions independently of the length of TTAGGG repeats and the G-strand overhang. *EMBO Rep.* 1:244–252.

Schotta, G., M. Lachner, K. Sarma, A. Ebert, R. Sengupta, G. Reuter, D. Reinberg, and T. Jenuwein. 2004. A silencing pathway to induce H3-K9 and H4-K20 trimethylation at constitutive heterochromatin. *Genes Dev.* 18:1251–1262.

Wang, Y., R.J. Giannone, and Y. Liu. 2005. Telomere sister chromatid exchange in telomerase deficient murine cells. *Cell Cycle*. 4:1320–1322.

Zijlmans, J.M., U.M. Martens, S.S. Poon, A.K. Raap, H.J. Tanke, R.K. Ward, and P.M. Lansdorp. 1997. Telomeres in the mouse have large inter-chromosomal variations in the number of T2AG3 repeats. *Proc. Natl. Acad. Sci. USA*. 94:7423–7428.